

Multiphonon structure of high-spin states in ^{40}Ca , ^{90}Zr , and ^{208}Pb

N. Lyutorovich and V. Tselyaev

St. Petersburg State University, St. Petersburg, 199034, Russia

(Dated: January 23, 2023)

The method of description of the high-spin states, which was previously developed and applied for the states of this type in ^{208}Pb , is generalized for the case of the states having more complex multiphonon structure. In this method, the harmonic approximation with the renormalized phonons is used in which the phonons themselves are determined within the non-linear version of the model based on the random-phase approximation (RPA) and including both the RPA correlations and the beyond-RPA ones. The mean field and the residual interaction are derived within the framework of the self-consistent RPA from the energy-density functional of the Skyrme type. The method is applied for the analysis of the available experimental data in doubly magic ^{208}Pb and ^{40}Ca and in semi-magic ^{90}Zr .

I. INTRODUCTION

High-spin states in nuclei have been the subject of the experimental and theoretical investigations for a long time (see reviews [1–3]) and continue to be a topic of current interest, see, e.g., Refs. [4–9]. The most part of the data on the high-spin states refers to the non-magic nuclei, however the recent experiments and theoretical analysis show that there are also long series of high-spin states in magic and semi-magic nuclei [10–18]. At present, the high-spin states have been experimentally identified only in two doubly-magic nuclei, ^{208}Pb and ^{40}Ca , and in the semi-magic nucleus ^{90}Zr . The first observation of high-spin states in these nuclei has been made in ^{90}Zr in Ref. [19] where the states up to spin $I = 20$ were investigated and the shell-model (SM) calculations were performed. The large-scale SM calculations for rotational bands in ^{90}Zr were also presented in Refs. [18, 20] where previous experiments and calculations are also reviewed. At the same time, the close coexistence of spherical states having n-particle–n-hole (nph) configuration structure with deformed and superdeformed rotational bands in magic and semi-magic nuclei significantly complicates their theoretical description.

Experimental and theoretical studies of ^{40}Ca nucleus show a very complex structure of its excited states, where the spherical states and approximately five rotational bands, including normally deformed (ND) and superdeformed (SD) bands, exist [11, 13, 16, 21]. The studies show that the first and the second 0^+ excited states in this nucleus, i.e. ND and SD band-heads, have 4p4h and 8p8h configuration structures, respectively. Calculations for the ND and SD bands were performed in the cranked relativistic mean-field [11] and cranked HF or HFB [12, 16, 22] models. The SD-band properties were also studied in the framework of the cranking covariant density functional theory with pairing in the shell-model-like approach with conserved particle numbers [17]. The transition (not band-head) energies and quadrupole moments of the ND and SD bands were well reproduced in the large-scale SM calculations in Ref. [13]. It should be noted that, in all these methods, calculations overes-

timate the energy of the ND and SD band-head states. However, besides the ND and SD bands, there are many other states in ^{40}Ca which have not yet been described within the microscopic approach.

The doubly magic ^{208}Pb is of particular interest since many high-spin states have been experimentally assigned in this nucleus and since it is a conventional laboratory to test the theory. Very important new experimental data for ^{208}Pb up to spin $I = 30$ together with a theoretical analysis in the framework of the SM have been presented in Ref. [15]. The advantage of the SM calculations is that they allow one to take into account many complex configurations. However, the model of Ref. [15] is not self-consistent in particular because the single-particle (sp) energies used in the calculations were adjusted to reproduce the experimental spectra of the neighboring odd nuclei.

The self-consistent description of the high-spin states in ^{208}Pb has been presented in Ref. [23] within the renormalized time-blocking approximation (RenTBA) developed in Ref. [24]. The RenTBA is the non-linear version of the model based on the random-phase approximation (RPA) and including both the RPA correlations and the beyond-RPA ones. The main configuration space of the RenTBA consists of the 1p1h and 1p1h \otimes phonon configurations where the phonons are determined self-consistently from the non-linear RenTBA equations and thus include correlations beyond the RPA. The more complex configurations are included in the RenTBA in part due to the ground-state correlations (of the RPA type) and the non-linear effects (see [24] for more details). In Ref. [23] it was obtained that the uncoupled 1p1h \otimes phonon configurations are rather good approximation for the high-spin states in ^{208}Pb . However, in this model the correlations between the 1p1h components of the 1p1h \otimes phonon configurations are neglected. The inclusion of these correlations means the replacement of the 1p1h \otimes phonon configurations with the phonon \otimes phonon ones. The results of Ref. [23] show that the effect of this replacement can be noticeable. One can expect that this effect will increase at the increase of the spin of the state resulting in the increase of its configuration complexity.

The most elaborated approach in which the mul-

tiphonon configurations are included explicitly is the quasiparticle-phonon model (QPM) of Soloviev and co-workers (see [25–28] and references therein and also Refs. [29, 30] where the self-consistent version of this model was developed). In the QPM, the interaction between the phonons is taken into account, but the phonons are determined as the solutions of the RPA or the quasiparticle RPA equations. More recently, the multiphonon models were developed in Refs. [31–33] within the framework of an equation of motion phonon method (EMPM), in which the phonons are introduced in the Tamm-Dancoff approximation, and in Ref. [34] within the covariant nuclear response theory based on the relativistic quasiparticle time-blocking approximation. However, to our knowledge, these models including QPM were not applied to the study of the multiphonon high-spin states.

Consistent multiphonon model should certainly takes into account interaction between the phonons and restrictions imposed by the Pauli principle. The phonon-phonon interaction is especially important in the models in which the phonon basis is fixed as it takes place, e.g., in the QPM and EMPM. In this case the phonon-phonon interaction can affect the properties of both multiphonon and one-phonon states, in particular, their energies. In the method used in Ref. [23], the effect of the phonon-phonon interaction on the one-phonon states is incorporated by means of the phonon renormalization within the RenTBA. The effect of this interaction on the two-phonon high-spin states (composed of the *renormalized* phonons) was found to be small by comparing the energies of the pure $1p1h \otimes$ phonon configurations with the results of the full-scale RenTBA calculations.

The goal of the present paper is to extend the method of Ref. [23] to the high-spin states having multiphonon structure. The calculation scheme is fully self-consistent and is based on the energy-density functional (EDF) of the Skyrme type. Calculations are performed for the high-spin states in ^{40}Ca , ^{90}Zr , and ^{208}Pb . The results are compared with available experimental data.

II. THEORETICAL FRAMEWORK AND CALCULATION SCHEME

Our approach is based on the harmonic approximation with the renormalized phonons. Thus, the basic elements of the theory are the phonons which are determined within the RenTBA. The RenTBA (see [24] for more details) is a non-linear version of the time-blocking approximation which is a model of the extended RPA type including $1p1h \otimes$ phonon configurations on top of the configurations incorporated in the RPA. The renormalized phonons are described by the solutions of the (non-linear) RenTBA equations and therefore include $1p1h$, $1p1h \otimes$ phonon, and more complex configurations resulting from the non-linear effects. As was shown in [24, 35], the renormalization reduces the energies of the phonons as compared to their RPA values that usually decreases

discrepancy with the experiment in the case of the self-consistent scheme based on the Skyrme EDFs, see Tables VII–IX in the Appendix. The harmonic approximation means that the interaction between $1p1h$ and more complex configurations is taken into account in the renormalized phonons (having relatively low energies) but not between them in the multiphonon configurations at higher energies and thus the energy of the multiphonon state is determined as a simple sum of the energies of the renormalized phonons. In what follows, we call this approach the multiphonon model in the harmonic approximation, or, for brevity, the multiphonon model. To minimize violation of the Pauli principle in the multiphonon configurations we use a simple method in which incompatible phonon combinations are excluded with the help of the numerical analysis of the $1p1h$ structure of the main (RPA) components of the phonons.

The technical details of the calculations are the following. The single-particle (s.p.) basis and residual interaction were calculated by the variational method for the Skyrme EDF as described in Ref. [36]. At the first step, the phonons are calculated in the RPA and, at the second step, they are self-consistently optimized in the RenTBA that implies the solution of the system of non-linear equations [24].

In the calculations, the Skyrme EDF with the parameter set SV-bas_{-0.44} was used. This set were obtained in Ref. [35] on the base of the parametrization SV-bas [37] to reproduce the basic experimental characteristics of the $M1$ excitations in ^{208}Pb within the RenTBA and at the same time to describe the nuclear ground-state properties with approximately the same accuracy as the original SV-bas set.

Wave functions and fields were represented on a spherical grid in coordinate space. The s.p. basis was discretized by imposing box boundary condition with a box radius equal to 18 fm. The particle's energies ε_p were limited by the maximum value $\varepsilon_p^{\text{max}} = 100$ MeV. The details of solving the non-linear RenTBA equations are described in Ref. [35].

III. RESULTS AND DISCUSSION

The high-spin states are in the energy region where the level density is high, so there may be uncertainties in comparing the theoretical values with the data. The uncertainties are not very essential in the given investigation because we consider only low levels for every spin and parity. For ^{208}Pb and ^{90}Zr , we study yrast, yrare, and those additional levels for which experimental data are available. For ^{40}Ca , where both spherical and deformed states are known, we investigate all the states excluding the ND and SD rotational bands because the method can not describe the states having a large deformation. At the same time, for ^{40}Ca and ^{90}Zr , we also considered states with low spins in order to give a complete picture of the states in these nuclei. The number

of known low-spin states in ^{208}Pb is very large, so they deserve a separate study which goes beyond the scope of this article.

A. ^{208}Pb

The results for the high-spin states in ^{208}Pb and a comparison with available data are presented in Tables I (positive parity states) and II (negative parity states), where I and π denote spin and parity of a state, n is a number of the level for the given I^π , E are experimental and theoretical energies (in MeV). The experimental values were taken from Refs. [15, 38]. The letters next to the theoretical values denote the phonon configuration for every multiphonon state. The correspondence of these letters to phonons and the structure of the RPA phonons are shown in the Appendix, Table VII. The renormalized phonons have more complex form where the RPA state presents the main part and, in addition, there are many additional components. Thus, the RPA phonon structure reflects the most significant part of the renormalized phonons. The renormalization of phonons changes the phonon energies of ^{208}Pb by 0.3 – 1.4 MeV, see Appendix, Table VII, and the renormalization is especially large for high-spin phonons.

In some cases, the spin-parity assignment of levels does not match in Refs. [15] and [38], namely, for the levels of 7.974, 8.027, and 9.061 MeV. In these cases, we preferred the [15] identification, because it is more recent and more substantiated. Our calculations confirm the correctness of this choice.

Tables I and II show that results of the self-consistent calculations for ^{208}Pb in the framework of the multiphonon model are in fairly well agreement with the experimental data without any refit of the parameters. The close results were obtained in Ref. [23] with parametrization SKXm $_{-0.49}$ [35], but here we extend the results to the three-phonon states. An important point is that, while there are many close two- and three-phonon states, the yrast and yrare nuclear levels are described just as the lowest states for the given spin and parity. Of course, the model cannot establish a one-to-one correspondence between theoretical and experimental values for these states. But for the yrast and yrare levels, the energies are predicted with an accuracy no worse than the difference between the energies of these levels.

The energies of the yrast states in ^{208}Pb as a function of $I(I+1)$ in the spin range $13 \leq I \leq 30$ are presented in Fig. 1. Here, the energies E (in MeV) calculated in the multiphonon model with the SV-bas $_{-0.44}$ functional are shown by green dots connected by lines of the same color, the experimental data [15, 38] are given in black squares.

Our new results confirm the conclusions made in the previous paper, Ref. [23]. The general trend looks very much like a rotational band, though the experimental trend in detail does not always follow exactly a straight

TABLE I. Positive parity states in ^{208}Pb obtained in the multiphonon model with renormalized phonons for the SV-bas $_{-0.44}$ Skyrme parametrization. Here, I^π denotes spin and parity of a level, n is a number of the level for the given I^π , E are experimental [15, 38] and theoretical energies. The letters next to the theoretical values denote phonons: see Appendix, Table VII.

I_n^π	$E[\text{MeV}]$		I_n^π	$E[\text{MeV}]$	
	Exp.	SV-bas $_{-0.44}$		Exp.	SV-bas $_{-0.44}$
14_1^+		9.16 bc	13_1^+		9.00 bc
14_2^+		9.36 cc	13_2^+		9.21 dj
16_1^+		9.21 bc	15_1^+	a	9.21 bc
16_2^+		9.35 cc	15_2^+		9.33 cc
18_1^+	9.1030	9.44 cc	17_1^+	9.061 a	9.43 cc
18_2^+		9.82 ck	17_2^+		9.68 ar
20_1^+	10.1959	9.51 cc	19_1^+	9.394	9.48 cc
(20_2^+)	10.3573	10.19 ck	(19^+) b	10.1358	10.04 ck
20_3^+	10.3710	10.63 cl	19^+	10.1362	10.17 cu
(20_4^+)	10.5313	10.64 cm	21_1^+		9.50 cc
(20_5^+)	10.5524	10.95 kl	21_2^+		10.38 ck
22_1^+		10.96 cl	23_1^+	11.3609	12.17 ll
22_2^+		11.60 ll	23_2^+		12.90 pr
24_1^+	11.9582	12.96 rr	25_1^+	12.9493	13.14 qr
24_2^+		13.00 qr	25_2^+		13.29 rr
26_1^+		13.11 rr	27_1^+		13.28 kk
26_2^+		13.30 qr	27_2^+		14.06 ccc
28_1^+		14.20 ccc	29_1^+		14.23 ccc
28_2^+		14.61 cck	29_2^+		14.60 cck
30_1^+		14.24 cc			
30_2^+		14.89 ccg			

^a The spin-parity assignment to the level 9.061 is (17^+) in the NDS [38] and 17^+ in Ref. [15] but 15^+ in Ref. [39].

^b The spin-parity assignment to the level 10.1358 in Ref. [15] is $(18^-, 19^+)$.

line: E is approximately constant in the ranges $I = 17 - 18$ and $26 - 28$. This deviation is easily explained in the framework of the multiphonon model. These parts with the constant E values arise as parts of the phonon multiplets with some additional details arisen because of the phonon renormalization. Nevertheless, on the whole, both experimental and theoretical trends are similar to a rotational band. However, this band does not rely on a collective rotation that is hindered by the spherical shape and the large shell gap in ^{208}Pb . The analysis of the microscopic structure shows that the high-spin states in ^{208}Pb have predominantly simple form in terms of s.p. excitations since these states have a simple form in terms of phonons (i.e., they are two- and three phonon states) and, at the same time, the phonons are approximately 1p1h states (see the in Table VII). Some complication arises because of the renormalization of the phonons, but this is just the same renormalization that changes the bare phonons appearing in the self-consistent RPA to the dressed phonons appearing as the ^{208}Pb lower spin states observed in the experiment. The rotational trend stems from a change in the angular momentum of one single

TABLE II. The same as in Table I but for the negative parity states in ^{208}Pb .

I_n^π	$E[\text{MeV}]$		I_n^π	$E[\text{MeV}]$	
	Exp.	SV-bas $_{-0.44}$		Exp.	SV-bas $_{-0.44}$
13_1^-	6.448	6.47 r	14_1^-	6.743	6.81 r
13_2^-	7.5288	7.62 ac	14_2^-	7.974 ^b	7.72 ac
15_1^-	8.027 ^a	8.34 cd	16_1^-	8.562	8.70 ce
(15_2^-)	8.1506	8.66 ce	16_2^-	8.6007	9.03 cd
15_3^-	8.2645	8.86 cf	16_3^-	8.7235	9.06 cf
15_4^-	8.3508	9.04 dk	18_1^-	10.1358 ^c	10.29 ci
17_1^-	8.8128	9.36 ch	18_2^-		10.35 cj
17_2^-		9.57 ct	20_1^-	10.3419	11.07 cp
19_1^-		10.55 cj	20_2^-		11.13 cr
19_2^-		11.03 br	22_1^-		11.22 cr
21_1^-	10.9343	11.15 cr	22_2^-		11.35 cq
21_2^-		11.22 co	24_1^-		11.47 cr
23_1^-		11.40 cr	24_2^-		12.28 lr
23_2^-		11.77 cs	26_1^-	13.5360	13.35 cce
25_1^-		12.87 lr	26_2^-		13.88 ccg
25_2^-		13.30 cce	28_1^-	13.6747	14.93 cci
27_1^-		14.08 ccg	28_2^-		15.00 ccp
27_2^-		14.22 cct	30_1^-		15.72 ccp
29_1^-		15.20 ccj	30_2^-		15.78 ccr
29_2^-		15.68 bcr			

^a The NDS [38] assignment to the level 8.027 is (14^-) but Ref. [15] defines this level as 15^- .

^b The NDS [38] spin-parity assignment to the level 7.974 is (15^-) but [15] assigns this level as 14^- .

^c The spin-parity assignment to the level 10.1358 in Ref. [15] is $(18^-, 19^+)$.

nucleon. Here the rotational part of the s.p. kinetic energy gives a large contribution to the nucleon energy and thereby to the change of nucleus energy.

The calculations show the following structure of the high-spin states in ^{208}Pb . The 13_1^- and 14_1^- states have one-phonon configurations while the other states with spins $13 \leq I \leq 26$ including 13_2^- and 14_2^- but except for 26^- are two-phonon configurations. The 26_2^+ and 27_1^+ states are of the two-phonon nature while all the other states with $I = 27$ and the even larger I need the treatment in terms of the three-phonon configurations. Of course, we described here only several lowest states for every spin and parity. For higher energies, the structure of states becomes more complicated.

B. ^{40}Ca

As it was mentioned, we do not consider the ND and SD rotational bands in ^{40}Ca based on the 0_2^+ and 0_3^+ states. The ND and SD band-head states have, in the deformed basis, the $4p4h$ and $8p8h$ configuration structure, respectively, and it is very difficult to describe such states in the spherical basis. The results for all other states in ^{40}Ca are presented in Tables III (positive parity states) and IV (negative parity) where denotations

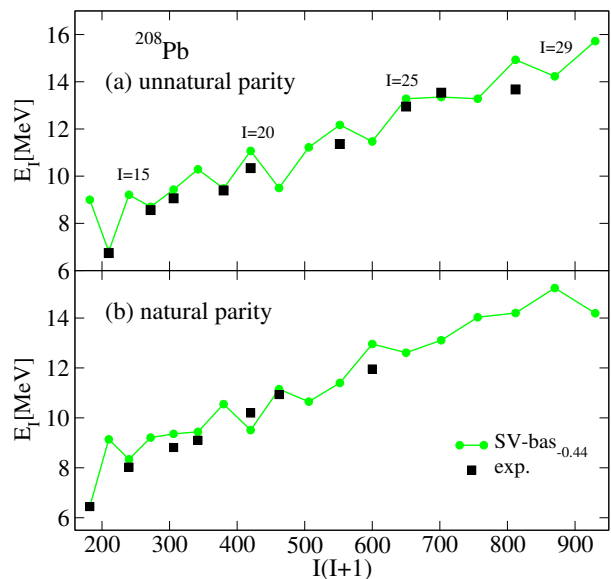


FIG. 1. The energies E_1 of ^{208}Pb yrast states calculated with RenTBA multiphonon model for the SV-bas $_{-0.44}$ Skyrme parametrization (green line with circles) are shown as function of $I(I+1)$ for the spins $13 \leq I \leq 30$ and compared with available experimental data [15, 38] (black squares).

are the same as in Table I, but different notation for phonons. The correspondence of the letters to phonons and the structure of the RPA phonons are shown in Appendix, Table VIII. The calculations were performed with the same SV-bas $_{-0.44}$ Skyrme parametrization that was used for ^{208}Pb . For ^{40}Ca , the renormalization of phonons changes the phonon energies by 0.2 – 0.6 MeV (see Appendix, Table VIII) that is less than the renormalization for ^{208}Pb . But many states in ^{40}Ca have 3-, 4- and even 5-phonon configurations therefore the renormalization can change the state energies by 1–1.5 MeV.

When evaluating the quality of the description of levels, two circumstances should be taken into account. First of all, our calculations are a first attempt to describe all these level in a self-consistent model. As shown in Introduction, there are calculations only for the ND and SD bands and all the calculations overestimate the energy of the band-heads by 2 MeV or more, therefore, in many papers, this energy or an energy of another band state (e.g., the $I = 16$ state in Ref. [17]) is taken as a reference. Secondly, we include in the consideration three rotational bands that have the following possible interpretation (see Ref. [21], p. 211 and references therein): γ sequence based on 8^+ state, 3^+ band, and $Kp = 0^-$ band (denotations [21]). The most deviation of our results from the data are just for the states of these bands but the deviation does not exceed 2 MeV and does not exceed the above mentioned deviation for the ND and SD band. Nevertheless, for some states of the three bands our results are in general satisfactory and may be considered as another possible interpretation of the states.

TABLE III. The same as in Table I but for the positive parity states in ^{40}Ca . The letters next to the theoretical values denote phonons: see Appendix, Table VIII. The experimental data are taken from Ref. [21].

I_n^π			I_n^π		
$E[\text{MeV}]$			$E[\text{MeV}]$		
Exp.		SV-bas $_{-0.44}$	Exp.		SV-bas $_{-0.44}$
2_2^+	5.249	6.75 aa	1_1^+		8.25 ac
2_4^+	6.422	8.25 ac	1_1^+		8.50 ad
4_2^+	6.507	6.75 aa	3^+	6.030 ^b	8.25 ac
$3^+, 4^+$	7.446	8.25 ac	3^+		8.38 ad
4^+	7.561	8.50 ad	(5^+)	7.397 ^b	8.25 ac
(6^+)	7.676	6.75 aa	5^+		8.38 ad
(6^+)	8.701	8.25 ac	(7^+)	8.936	8.25 ac
8^+	8.100 ^a	8.38 ad	7^+		8.38 ad
8^+		9.73 cc	(9^+)	11.70	9.87 cd
10^+	11.00 ^a	13.5 aaaa	9^+		10.12 ce
(10^+)	12.59	15.0 aaac	(11^+)	13.53 ^b	15.0 aaac
(10^+)	13.19	15.13 aaad	11^+		15.1 aaad
(12^+)	13.12 ^a	15.0 aaac	(13^+)	15.15 ^a	15.1 aaad
(12^+)	15.75	15.1 aaad	(13^+)	16.58 ^b	16.5 aacc
(14^+)	17.70	16.9 aade	(15^+)	19.19	18.13 aadf
(14^+)	18.05	17.0 aae	(15^+)		18.25 aaef
(14^+)	18.72	18.0 aacf			

^a γ sequence based on 8^+ [21], p. 211.

^b 3^+ band [21], p. 211.

The one-phonon $E(0_1^-)$ and $E(1_1^-)$ values exceed the proton separation energy in ^{40}Ca calculated with the given parameter set, $S_{\text{theor.}}(p) = 7.565$ MeV (the experimental value $S_{\text{exp.}}(p) = 8328.17$ [21]). These energies have been recalculated in RenTBA taking into account the s.p. continuum, and the values given in the tables takes this effect into account. The continuum effect is not significant for the two- and many-phonon states.

The calculation results allow us to refine the identification of some levels in ^{40}Ca . The experimental assignment to the 7.623 level is $(2^-, 3, 4^+)$ [21]. Possible theoretical states corresponding to this level are 2_5^- , 3_5^- , 3_2^+ , and 4_7^+ with the energies 8.77, 7.45 k, 8.38 ad and 8.63 ab, respectively. It should be noted that the 4_1^+ and 4_3^+ states belong to the ND and SD bands, respectively, and therefore they are not shown in the table. The most probable assignment for the 7.623 level is 3_5^- .

The experimental assignment to the 6.938 level is $(1^-$ to $5^-)$ [21] but our calculations show that the most probable assignment is 5^- because all the other states have too high energies. The experimental assignment to the 8.359 level is $(0, 1, 2)^-$ [21]. Our calculations show that the most probable assignment is 0_1^- .

C. Semi-magic ^{90}Zr

New experimental data for the states up to spin $I = 20$ in ^{90}Zr and the shell-model calculations are given in Ref. [18]. The ^{90}Zr high-spin states were interpreted to be

TABLE IV. The same as in Table III but for the negative parity states in ^{40}Ca .

I_n^π			I_n^π		
$E[\text{MeV}]$			$E[\text{MeV}]$		
Exp.		SV-bas $_{-0.44}$	Exp.		SV-bas $_{-0.44}$
$(0, 1, 2)^-$	8.359 ^a	8.40	1^-	5.903	7.62 l
2^-	6.025	5.33 d	3^-	3.737	3.38 a
2^-	6.750	6.29 f	(3^-)	6.160	5.25 b
4^-	5.613	4.87 c	3^-	6.285	5.70 i
4^-		5.12 e	3^-	6.582	7.14 j
(6^-)	8.701	10.13 aaa	$(2^-, 3, 4^+)$	7.623 ^b	7.45 k
6^-		11.62 aac	5^-	4.491	5.00 d
8^-	10.47	11.62 aac	5^-	6.938 ^c	6.37 f
8^-		11.76 aad	(7^-)	9.033? ^d	10.13 aaa
(10^-)	13.19	11.76 aad	7^-	11.69	11.62 aac
10^-		11.87 aae	(9^-)	10.89 ^d	11.62 aac
12^-		13.25 acd	(11^-)	12.92 ^d	11.76 aad
12^-		13.50 ade	11^-		13.11acc
14^-		16.25 cdf	(13^-)	15.31 ^d	14.8 adf
14^-		16.38 ddf	(13^-)	16.58 ^e	15.0 cde
			(15^-)	18.21 ^d	18.51 aaaa

^a The experimental assignment to the 8.359 level is $(0, 1, 2)^-$ [21] but our calculations show that the most probable assignment is 0_1^- : see the text.

^b The experimental assignment to the 7.623 level is $(2^-, 3, 4^+)$ [21] but our calculations show that the most probable assignment is 3_5^- .

^c The experimental assignment to the 6.938 level is $(1^-$ to $5^-)$ [21] but our calculations show that the most probable assignment is 5^- .

^e A possible interpretation of the level as a member of the band as $Kp = 0^-$ band and some doubts on this interpretation are given in Ref. [21], p. 211.

^d 3^+ band [21], p. 211.

generated by the recoupling of stretched proton and neutron configurations. The shell-model calculations [18] used the fitted s.p. energies and two-body matrix elements of the effective interaction. Besides the two bands considered in Ref. [18], there are many other known levels in ^{90}Zr having both the low and high spins. The calculations presented in this subsection are the first attempt to describe all known states of ^{90}Zr within the framework of a self-consistent method.

The results for ^{90}Zr are shown in Tables V (positive parity states) and VI (negative parity) where denotations are the same as in Table I, but different notation for phonons. The correspondence of the letters to phonons and the structure of the RPA phonons are shown in Appendix, Table IX. The experimental data are taken from Refs. [18, 40].

It should be noted that there are many unassigned levels above 3.5 MeV, such as 3.557 MeV, 3.9324 MeV, etc. [40], so it is possible that some of the lowest assigned levels are not yrast or yrare. This should be taken into account when comparing theory with data, since the theoretical values are given just for the yrast and yrare states.

The calculations with the SV-bas $_{-0.44}$ parameter set

TABLE V. The same as in Table I but for the positive parity states in ^{90}Zr . The letters next to the theoretical values denote phonons: see Appendix, Table IX. The experimental data are taken from Ref. [18, 40]. The theoretical results were obtained with SV-bas $_{-0.44}$ and SLy4 Skyrme EDF parametrizations but, for SV-bas $_{-0.44}$ (denoted as bas $_{-0.44}$), the energy of the single-particle $\pi 1g_{9/2}$ state was increased by 0.6 MeV in these calculations.

I_n^π	$E[\text{MeV}]$			I_n^π	$E[\text{MeV}]$		
	exp.	bas $_{-0.44}$	SLy4		exp.	bas $_{-0.44}$	SLy4
0^+	1.76	3.67 ^x	4.27 aa ^x	1^+	3.67	4.28 aa	
0^+	4.12	5.03	5.68 ab	1^+	5.96	5.75 ab	
0^+	4.43	5.19	5.77 bb				
2^+	2.19	3.60 ^x	4.27 aa ^x	(3^+)	4.26	3.67	4.28 aa
2^+	3.31	3.67	4.31 d	3^+	3.84	4.94 d	
2^+	3.84	4.93	5.46 ab				
2^+	4.22	5.81	5.77 bb				
2^+	4.23	5.90	5.97 ac				
4^+	3.08	3.67	4.27 aa	(5^+)	4.45	3.67	4.28 aa
4^+	4.06	3.68	4.70 d	5^+	4.87	3.81	4.89 d
4^+	4.30	5.02	5.02 ab	7^+	^a 3.67	4.28 aa	
4^+	4.33	5.25	5.77 bb	7^+	5.06	4.03	4.75d
(4^+)	4.35	5.89	5.79 ab	9^+	5.25	3.67	4.28 aa
4^+	4.47	5.90	6.18 ac	9^+	5.79	5.08	5.83 ab
6^+	3.45	3.62	4.27 aa	11^+	6.28	6.10	6.12 ac
6^+		3.74	4.88 d	(11^+)	7.19	6.53	7.42 bb
8^+	3.59	3.67	4.27 aa	13^+	7.44	7.46	8.01 cc
8^+	5.16	5.00	5.02 ab	13^+		8.36	9.10 aad
10^+	5.64	5.11	5.83 ab	15^+	8.95	8.56	9.24 aad
10^+	7.03	5.84	6.10 ac	15^+	9.33	8.93	10.4 abd
(12^+)	6.77	7.44	7.77 bc	(15^+)	9.84	9.54	10.9 acd
12^+	7.22	7.49	7.99 cc	(17^+)	10.8	9.10	10.6 abd
14^+	8.06	7.52	9.07 aad	17^+		9.92	10.9 acd
14^+		8.85	10.2 abd	(19^+)	12.1	11.6	12.5 bcd
16^+	^b	7.65	8.90 aad	19^+		11.5	12.6 aabd
16^+	10.1	8.92	10.6 abd				
(18^+)	11.4	10.1	10.9 acd				
18^+		10.7	12.2 bbc				
(20^+)	13.0	11.5 ^c	12.8 ccd				
20^+		12.7 ^c	13.7 aadd				

^a The 7^+ state belongs to the 'aa' multiplet where the known 2_1^+ , 4_1^+ , 6_1^+ , and 8_1^+ members have energies of 2.5 – 3.5 MeV so there should be a 7^+ state with an energy of 3 – 4 MeV. The same is valid for the 'd' multiplet.

^b The level 10.12584 [40] cannot be the first state of 16^+ ; it's either 2nd or 3rd: see the text.

^c For SV-bas $_{-0.44}$, the first and second have the configurations 'aadd' and 'ccd', respectively.

^x The first 0^+ and 2^+ state are probably deformed and therefore outside the scope of the model: see the text.

underestimate energies of many states in ^{40}Ca by 2 – 4 MeV, particularly for the high-spin states. At the same time, it turns out that a small change in only one s.p. energy, for the $\pi 1g_{9/2}$ state, significantly improves agreement with experiment. The SV-bas $_{-0.44}$ results given in Tables V and VI were obtained with the energy of the $\pi 1g_{9/2}$ state increased by 0.6 MeV. This feature of the calculations is designated in Tables V and VI as bas $_{-0.44}$.

TABLE VI. The same as in Table V but for the negative parity states in ^{90}Zr .

I_n^π	$E[\text{MeV}]$			I_n^π	$E[\text{MeV}]$		
	exp.	bas $_{-0.44}$	SLy4		exp.	bas $_{-0.44}$	SLy4
0^-		5.59	6.93 ad	1^-		5.60	5.00 ad
0^-		6.75	7.79 aab	1^-		6.79	5.59 bd
2^-		4.53	4.83 c	3^-	2.75	2.60	2.88 b
2^-		5.60	6.88 ad	(3^-)	4.50	3.84	3.97 c
(4^-)	2.74	1.89	2.26 a	(3^-)	4.81	5.62	5.86 h
(4^-)	4.22	3.24	3.78 b	3^-	5.63	6.01	6.66 ad
(4^-)	4.54	4.00	4.10 c	3^-	5.67	6.66	7.46 aab
(4^-)	4.94	5.75	6.82 ad	5^-	2.32	1.78	2.02 a
6^-	4.23	3.38	3.76 b	5^-	3.96	3.14	3.66 b
6^-		3.87	3.95 c	(5^-)	4.30	3.90	3.88 c
8^-		5.64	6.94 ad	7^-	4.37	4.49	4.06 c
8^-		6.72	7.64 bd	7^-		5.63	6.84 ad
10^-	6.38	5.70	6.96 ad	9^-		5.66	6.97 ad
10^-	6.72	6.72	7.64 bd ^a	9^-		6.66	7.55 aab
(12^-)		5.81	6.77 ad	11^-	6.95	5.75	6.89 ad
12^-		6.90	7.79 aab	11^-	7.01	6.77	7.53 aab
14^-	8.86	7.78	8.22 aac	13^-		6.91	7.81 aab
14^-		8.40	8.81 cd	13^-		7.41	8.50 bd
(16^-)	9.71	10.1	10.1 acc	15^-	8.96	9.10	9.63 abc
(16^-)	10.0	10.6	11.5 bbc	15^-	9.83	9.87	10.10 acc
16^-	10.1	10.7	11.6 bcc	15^-	9.97	10.3	10.63 bcc
16^-	10.4	11.1	11.7 add	17^-	10.8	9.58	11.69 add
18^-	11.3	9.55	11.6 add	17^-	10.9	10.6	11.69 bcc
18^-	11.4	11.2	12.0 ccc				
20^-	12.6	12.2	12.8 aacd	19^-	12.1	11.2	12.5 aabd
20^-	13.0	12.3	13.7 cdd	19^-	12.3	12.1	12.8 aacd

^a The 'bd' and 'aab' configurations have very close energies for the 8_2^- level; the same is also for 10_2^- .

To keep full self-consistency of the method, we also performed calculations for ^{90}Zr with the well known forces SLy4. It is interesting to note, that the self-consistent SLy4 results for many levels are rather close to the bas $_{-0.44}$ values calculated with this increased $\pi 1g_{9/2}$ energy.

The result for ^{90}Zr presented in the tables are in general acceptable, particularly, taking into account the high sensitivity to the EDF parameters. The most significant deviations are for the first excited 0^+ and 2^+ states, i. e. 0_2^+ and 2_1^+ , but these states have, probably, a large deformation. The experimental ratio

$$\frac{E(4_1^+) - E(0_2^+)}{E(2_1^+) - E(0_2^+)} = 3.07 \quad (1)$$

is very close to the rotational limit 3.33. The deformed states are beyond the scope of the model using the spherical basis but for completeness we include the 0^+ levels of ^{90}Zr in the table.

At the same time, unlike ^{40}Ca , the deformation manifested in the 0_2^+ , 2_1^+ and, may be, 4_1^+ states in ^{90}Zr is not

seen in the 6_1^+ state, since the experimental ratio

$$\frac{E(6_1^+) - E(0_2^+)}{E(2_1^+) - E(0_2^+)} = 3.93 \quad (2)$$

is significantly less than the rotational value of 7.00. All the result for ^{90}Zr , excluding 0_2^+ and 2_1^+ states, are in a better and sometimes in nice agreement with the data.

One can expect that these results can serve as a guideline for the search of the new states in ^{90}Zr . For example, the 6_1^+ , 7_1^+ , and 8_1^+ levels are a part of the 'aa' multiplet where the 6_1^+ and 8_1^+ states have the experimental values of energies are 3.45–3.59 MeV, so there should be a state 7^+ , which has approximately the same energy and this state should be yrast. Therefore the experimental 5.060 level is placed as the second 7^+ state in Table V. The states 14^+ and 16^+ are a part of the "aad" multiplet, so there must be a level 16_1^+ that is close in energy to the level 14^+ with $E(14^+) = 8.058$ MeV. Therefore, 10.12584 cannot be the yrast state of 16^+ ; it's either 2nd or 3rd state.

IV. SUMMARY AND CONCLUSIONS

In the paper, the self-consistent calculations of the structure and energies of the high-spin states in doubly magic ^{208}Pb and ^{40}Ca and in semi-magic ^{90}Zr have been presented. The calculations were performed within the framework of the multiphonon model including the renormalized phonons in the harmonic approximation and based on the energy-density functional (EDF) of the Skyrme type. The basic elements of the theory, the phonons, are determined within the renormalized time-blocking approximation which is a non-linear version of the model of the beyond-RPA type.

In ^{208}Pb , the calculations have been performed for all the experimentally known levels of spins $I \geq 13$ and, when there are no data, for all yrast and yrare states of $13 \leq I \leq 30$. In ^{40}Ca and ^{90}Zr , the results have been obtained for all the experimentally known high-spin states which can be described within our approach based on the spherically-symmetric mean field. The results for ^{208}Pb are in fairly well agreement with the experimental data despite the fact that no new fitting parameters in the underlying Skyrme EDF were introduced. The results for ^{40}Ca and ^{90}Zr are less satisfactory with respect to comparison with data, but in part it is explained by the parametrization of the Skyrme EDF used in all the calculations and adjusted previously to the properties of the excited states of ^{208}Pb .

The choice of the EDF is important in describing the multiphonon states because of their sensitivity to the parameters of the EDF which affect the phonon's energies. This is demonstrated in the case of ^{90}Zr . A change in one phonon causes much more significant change in the n-phonon energy. At the same time, there are many high-spin states having rather simple structure in terms of the

renormalized phonons. Therefore the energies of the multiphonon states can be used as the additional fit data for adjustment of the parameters of the EDFs.

Our results confirm the conclusion of Ref. [23] about importance of the use of the renormalized phonons in the description of the high-spin states. The renormalization reduces the phonon's energies that in the most cases improves agreement with data.

ACKNOWLEDGMENTS

This work was supported by the Russian Foundation for Basic Research, project number 21-52-12035. This research was carried out using computational resources provided by the Computer Center of St. Petersburg State University.

Appendix A: Phonons

Structure and energies of the phonons used in the calculations of the multiphonon states in ^{208}Pb are shown in Table VII for the SV-bas_{-0.44} Skyrme parameter set. Here, the last two columns show the energies of the RPA and RenTBA (renormalized) phonons. The letters a, b, c, ... denote multiplets of phonons having approximately the same structure.

Tables VIII and IX show the structure and energies of the phonons for ^{40}Ca and ^{90}Zr , respectively.

TABLE VII. Structure and energy (in MeV) of some phonons appearing in the n-phonon states of ^{208}Pb . The last three columns show the experimental data [38, 41] and the energies of the RPA and RenTBA (renormalized) phonons. The letters a, b, c, ... denote multiplets of phonons having approximately the same structure.

	I^π	Configuration	$E[\text{MeV}]$		
			Exp.	RPA	RenTBA
a	3_1^-	$\nu 2g_{9/2} 3p_{3/2}^{-1} 21\% + \pi 1h_{9/2} 2d_{3/2}^{-1} 20\% + \dots$	2.614	3.10	2.87
b	2_1^+	$\nu 2g_{9/2} 1i_{13/2}^{-1} 63\% + \pi 2f_{7/2} 1h_{11/2}^{-1} 19\%$	4.086	4.42	4.01
	4_1^+	$\nu 2g_{9/2} 1i_{13/2}^{-1} 58\% + \pi 1h_{9/2} 1h_{11/2}^{-1} 16\%$	4.324	4.80	4.31
	6_1^+	$\nu 2g_{9/2} 1i_{13/2}^{-1} 64\% + \pi 1h_{9/2} 1h_{11/2}^{-1} 18\%$	4.424	5.13	4.56
c	5_1^+	$\nu 2g_{9/2} 1i_{13/2}^{-1} 99\%$	4.962	5.36	4.69
	7_1^+	$\nu 2g_{9/2} 1i_{13/2}^{-1} 98\%$	4.867	5.36	4.68
	8_1^+	$\nu 2g_{9/2} 1i_{13/2}^{-1} 92\%$	4.611	5.31	4.66
	9_1^+	$\nu 2g_{9/2} 1i_{13/2}^{-1} 99\%$	5.010	5.39	4.70
	10_1^+	$\nu 2g_{9/2} 1i_{13/2}^{-1} 98\%$	4.895	5.34	4.65
	11_1^+	$\nu 2g_{9/2} 1i_{13/2}^{-1} 100\%$	5.235	5.54	4.85
d	4_1^-	$\nu 2g_{9/2} 3p_{1/2}^{-1} 98\%$	3.475	4.15	3.65
	5_1^-	$\nu 2g_{9/2} 3p_{1/2}^{-1} 70\% + \pi 1h_{9/2} 3s_{1/2}^{-1} 18\%$	3.198	3.92	3.51
e	4_2^-	$\pi 1h_{9/2} 3s_{1/2}^{-1} 99\%$	3.947	4.36	3.93
	5_2^-	$\pi 1h_{9/2} 3s_{1/2}^{-1} 70\% + \nu 2g_{9/2} 3p_{1/2}^{-1} 24\%$	3.708	4.29	3.85
f	5_3^-	$\nu 2g_{9/2} 3p_{3/2}^{-1} 48\% + \pi 1h_{9/2} 2d_{3/2}^{-1} 28\%$	3.961	4.73	4.21
g	6_2^-	$\pi 1h_{9/2} 2d_{3/2}^{-1} 83\%$	4.206	5.05	4.58
h	6_3^-	$\nu 2g_{9/2} 2f_{5/2}^{-1} 79\%$	4.383	5.14	4.52
	7_1^-	$\nu 2g_{9/2} 2f_{5/2}^{-1} 97\%$	4.037	5.41	4.75
i	7_2^-	$\nu 1i_{11/2} 3p_{3/2}^{-1} 96\%$	4.680	6.00	5.44
j	8_1^-	$\nu 1i_{11/2} 2f_{5/2}^{-1} 99\%$	4.919	6.29	5.70
k	8_2^+	$\pi 1h_{9/2} 1h_{11/2}^{-1} 76\%$	4.861	5.74	5.15
	9_2^+	$\pi 1h_{9/2} 1h_{11/2}^{-1} 99\%$	5.162	5.73	5.15
	10_2^+	$\pi 1h_{9/2} 1h_{11/2}^{-1} 79\%$	5.069	6.11	5.53
l	9_3^+	$\nu 1i_{11/2} 1i_{13/2}^{-1} 98\%$	5.327	6.48	5.82
	10_3^+	$\nu 1i_{11/2} 1i_{13/2}^{-1} 82\% + \pi 1h_{9/2} 1h_{11/2}^{-1} 18\%$	5.537	6.72	6.01
	11_2^+	$\nu 1i_{11/2} 1i_{13/2}^{-1} 100\%$	5.750	6.46	5.80
	12_1^+	$\nu 1i_{11/2} 1i_{13/2}^{-1} 100\%$	5.864	7.05	6.37
m	9_4^+	$\pi 2f_{7/2} 1h_{11/2}^{-1} 94\%$	5.901	6.69	5.79
o	7_6^-	$\pi 1i_{13/2} 1h_{11/2}^{-1} 75\% + \nu 1j_{15/2} 1i_{13/2}^{-1} 21\%$, $X_1 > 0, X_2 > 0$		7.48	6.51
	9_1^-	$\pi 1i_{13/2} 1h_{11/2}^{-1} 99\%$	6.861	7.51	6.56
	11_1^-	$\pi 1i_{13/2} 1h_{11/2}^{-1} 96\%$		7.48	6.52
p	8_2^-	$\pi 1i_{13/2} 1h_{11/2}^{-1} 59\% + \nu 1j_{15/2} 1i_{13/2}^{-1} 37\%$, $X_1 > 0, X_2 > 0$	5.836	7.33	6.40
	10_1^-	$\pi 1i_{13/2} 1h_{11/2}^{-1} 53\% + \nu 1j_{15/2} 1i_{13/2}^{-1} 47\%$, $X_1 > 0, X_2 > 0$	6.283	7.39	6.42
q	12_1^-	$\nu 1j_{15/2} 1i_{13/2}^{-1} 68\% + \pi 1i_{13/2} 1h_{11/2}^{-1} 32\%$	6.435	7.52	6.49
r	11_2^-	$\nu 1j_{15/2} 1i_{13/2}^{-1} 96\%$		7.60	6.50
	13_1^-	$\nu 1j_{15/2} 1i_{13/2}^{-1} 100\%$		7.57	6.47
	14_1^-	$\nu 1j_{15/2} 1i_{13/2}^{-1} 100\%$	6.743	8.02	6.81
s	12_2^-	$\pi 1i_{13/2} 1h_{11/2}^{-1} 68\% + \nu 1j_{15/2} 1i_{13/2}^{-1} 32\%$, $X_1 > 0, X_2 < 0$	7.061	8.06	6.92
t	6_4^-	$\nu 1i_{11/2} 3p_{1/2}^{-1} 82\%$	4.481	5.21	4.72
u	8_3^+	$\nu 1j_{15/2} 3p_{1/2}^{-1} 83\%$	5.093	6.19	5.32
v	12_2^+	$\nu 1j_{15/2} 1h_{9/2}^{-1} 83\%$	a	10.37	8.95

^a The 12_2^+ state has a 2-phonon configuration and therefore its energy should not be compared with the 1-phonon energy.

TABLE VIII. The same as in Table VII but for ^{40}Ca . The experimental data are taken from Ref. [21].

I^π	Configuration	$E[\text{MeV}]$		
		Exp.	RPA	RenTBA
a	3_1^-	$\pi 1f_{7/2} 1d_{3/2}^{-1} 37\% + \nu 1f_{7/2} 1d_{3/2}^{-1} 30\% + \dots, X_1 > 0, X_2 > 0$		
b	3_2^-	$\pi 1f_{7/2} 1d_{3/2}^{-1} 52\% + \nu 1f_{7/2} 1d_{3/2}^{-1} 29\%, X_1 > 0, X_2 < 0$		
c	4_1^-	$\pi 1f_{7/2} 1d_{3/2}^{-1} 97\%$		
d	5_1^-	$\pi 1f_{7/2} 1d_{3/2}^{-1} 60\% + \nu 1f_{7/2} 1d_{3/2}^{-1} 39\%, X_1 > 0, X_2 > 0$		
	2_1^-	$\pi 1f_{7/2} 1d_{3/2}^{-1} 64\% + \nu 1f_{7/2} 1d_{3/2}^{-1} 36\%, X_1 > 0, X_2 > 0$		
e	4_2^-	$\nu 1f_{7/2} 1d_{3/2}^{-1} 96\%$		
f	2_2^-	$\nu 1f_{7/2} 1d_{3/2}^{-1} 61\% + \pi 1f_{7/2} 1d_{3/2}^{-1} 34\%, X_1 > 0, X_2 < 0$		
	5_2^-	$\nu 1f_{7/2} 1d_{3/2}^{-1} 59\% + \pi 1f_{7/2} 1d_{3/2}^{-1} 38\%, X_1 > 0, X_2 < 0$		
i	3_3^-	$\nu 1f_{7/2} 1d_{3/2}^{-1} 35\% + \nu 1f_{7/2} 2s_{1/2}^{-1} 33\% + \dots, X_1 > 0, X_2 > 0$		
j	3_4^-	$\nu 1f_{7/2} 2s_{1/2}^{-1} 44\% + \pi 1f_{7/2} 2s_{1/2}^{-1} 35\% + \dots, X_1 > 0, X_2 < 0$		
k	3_5^-	$\pi 2p_{3/2} 1d_{3/2}^{-1} 57\% + \nu 2p_{3/2} 1d_{3/2}^{-1} 36\%, X_1 > 0, X_2 > 0$		
l	1_1^-	$\pi 2p_{3/2} 1d_{3/2}^{-1} 55\% + \nu 2p_{3/2} 1d_{3/2}^{-1} 25\%, X_1 > 0, X_2 > 0$		

TABLE IX. The same as in Table VII but for ^{90}Zr . The calculation values are given for the SLy4 parameter set. The experimental data are taken from Refs. [18, 40].

I^π	Configuration	$E[\text{MeV}]$			I^π	Configuration	$E[\text{MeV}]$		
		Exp.	RPA	RenTBA			Exp.	RPA	RenTBA
a	4_1^-	$\pi 1g_{9/2} 2p_{1/2}^{-1} 100\%$			5_1^-	$\pi 1g_{9/2} 2p_{1/2}^{-1} 100\%$			
b	3_1^-	$\pi 1g_{9/2} 2p_{3/2}^{-1} 88\%$			4_2^-	$\pi 1g_{9/2} 2p_{3/2}^{-1} 98\%$			
	5_2^-	$\pi 1g_{9/2} 2p_{3/2}^{-1} 99\%$			6_1^-	$\pi 1g_{9/2} 2p_{3/2}^{-1} 98\%$			
c	2_1^-	$\pi 1g_{9/2} 1f_{5/2}^{-1} 99\%$			3_2^-	$\pi 1g_{9/2} 1f_{5/2}^{-1} 91\%$			
	4_3^-	$\pi 1g_{9/2} 1f_{5/2}^{-1} 98\%$			5_3^-	$\pi 1g_{9/2} 1f_{5/2}^{-1} 99\%$			
	6_2^-	$\pi 1g_{9/2} 1f_{5/2}^{-1} 97\%$			7_1^-	$\pi 1g_{9/2} 1f_{5/2}^{-1} 99\%$			
d	2_1^+	$\nu 2d_{5/2} 1g_{9/2}^{-1} 97\%$			3_1^+	$\nu 2d_{5/2} 1g_{9/2}^{-1} 99\%$			
	4_1^+	$\nu 2d_{5/2} 1g_{9/2}^{-1} 99\%$			5_1^+	$\nu 2d_{5/2} 1g_{9/2}^{-1} 99\%$			
	6_1^+	$\nu 2d_{5/2} 1g_{9/2}^{-1} 100\%$			7_1^+	$\nu 2d_{5/2} 1g_{9/2}^{-1} 100\%$			
h	2_2^+	$\nu 1g_{7/2} 1g_{9/2}^{-1} 97\%$							

- [1] M. J. A. de Voigt, J. Dudek, and Z. Szymański, *Rev. Mod. Phys.* **55**, 949 (1983).
- [2] J. X. Saladin, R. A. Sorensen, and C. M. Vincent, *High Spin Physics and Gamma-Soft Nuclei* (WORLD SCIENTIFIC, 1991) <https://www.worldscientific.com/doi/pdf/10.1142/1242>.
- [3] D. Ward and P. Fallon, "High spin properties of atomic nuclei," in *Advances in Nuclear Physics*, edited by J. W. Negele and E. W. Vogt (Springer US, Boston, MA, 2001) pp. 167–291.
- [4] J. Meng, S. Q. Zhang, and P. W. Zhao, in *Relativistic Density Functional for Nuclear Structure*, Vol. International Review of Nuclear Physics – Vol. 10, edited by J. Meng (World Scientific Publishing Co. Pte. Ltd., 2016)

- pp. 355–412.
- [5] S. Frauendorf, *Physica Scripta* **93**, 043003 (2018).
- [6] C. Petrache, P. Walker, S. Guo, Q. Chen, S. Frauendorf, Y. Liu, R. Wyss, D. Mengoni, Y. Qiang, A. Astier, E. Dupont, R. Li, B. Lv, K. Zheng, D. Bazzacco, A. Boso, A. Goasduff, F. Recchia, D. Testov, F. Galtarossa, G. Jaworski, D. Napoli, S. Riccetto, M. Siciliano, J. Valiente-Dobon, M. Liu, X. Zhou, J. Wang, C. Andreoiu, F. Garcia, K. Ortner, K. Whitmore, T. Back, B. Cederwall, E. Lawrie, I. Kuti, D. Sohler, J. Timar, T. Marchlewski, J. Srebrny, and A. Tucholski, *Physics Letters B* **795**, 241 (2019).
- [7] V. Kumar and P. C. Srivastava, *Nuclear Physics A* **1002**, 121989 (2020).

- [8] A. V. Afanasjev, “Model for independent particle motion,” in *Handbook of Nuclear Physics*, edited by I. Tanihata, H. Toki, and T. Kajino (Springer Nature Singapore, Singapore, 2022) pp. 1–40.
- [9] K. Yoshida, *Phys. Rev. C* **105**, 024318 (2022).
- [10] D. Rudolph, C. Baktash, M. J. Brinkman, E. Caurier, D. J. Dean, M. Devlin, J. Dobaczewski, P.-H. Heenen, H.-Q. Jin, D. R. LaFosse, W. Nazarewicz, F. Nowacki, A. Poves, L. L. Riedinger, D. G. Sarantites, W. Satuła, and C.-H. Yu, *Phys. Rev. Lett.* **82**, 3763 (1999).
- [11] E. Ideguchi, D. G. Sarantites, W. Reviol, A. V. Afanasjev, M. Devlin, C. Baktash, R. V. F. Janssens, D. Rudolph, A. Axelsson, M. P. Carpenter, A. Galindo-Uribarri, D. R. LaFosse, T. Lauritsen, F. Lerma, C. J. Lister, P. Reiter, D. Seweryniak, M. Weiszflog, and J. N. Wilson, *Phys. Rev. Lett.* **87**, 222501 (2001).
- [12] T. Inakura, S. Mizutori, M. Yamagami, and K. Matsuyanagi, *Nuclear Physics A* **710**, 261 (2002).
- [13] E. Caurier, J. Menéndez, F. Nowacki, and A. Poves, *Phys. Rev. C* **75**, 054317 (2007).
- [14] Y. Chiba and M. Kimura, *Phys. Rev. C* **89**, 054313 (2014).
- [15] R. Broda, R. V. F. Janssens, L. W. Iskra, J. Wrzesinski, B. Fornal, M. P. Carpenter, C. J. Chiara, N. Cieplicka-Oryńczak, C. R. Hoffman, F. G. Kondev, W. Królas, T. Lauritsen, Z. Podolyak, D. Seweryniak, C. M. Shand, B. Szpak, W. B. Walters, S. Zhu, and B. A. Brown, *Phys. Rev. C* **95**, 064308 (2017).
- [16] S. Sakai, K. Yoshida, and M. Matsu, *Progress of Theoretical and Experimental Physics* **2020** (2020), 10.1093/ptep/ptaa071, 063D02, <https://academic.oup.com/ptep/article-pdf/2020/6/063D02/33424844/ptaa071.pdf>.
- [17] F. Wang, Z. Shi, and X. W. Xia, *Phys. Rev. C* **102**, 014321 (2020).
- [18] P. Dey, D. Negi, R. Palit, P. C. Srivastava, M. S. R. Laskar, B. Das, F. S. Babra, S. Bhattacharya, B. Das, K. R. Devi, R. Gala, U. Garg, S. S. Ghugre, E. Ideguchi, S. Kumar, A. Kundu, G. Mukherjee, S. Muralithar, S. Nag, S. Nandi, Neelam, M. K. Raja, R. Raut, R. Santra, A. Sharma, S. Sihotra, A. K. Singh, R. P. Singh, and T. Trivedi, *Phys. Rev. C* **105**, 044307 (2022).
- [19] E. K. Warburton, J. W. Olness, C. J. Lister, R. W. Zurmühle, and J. A. Becker, *Phys. Rev. C* **31**, 1184 (1985).
- [20] H. Wang, K.-Y. Ma, S.-Y. Liu, and J.-B. Lu, *Chinese Physics C* **45**, 094106 (2021).
- [21] J. Chen, *Nuclear Data Sheets* **140**, 1 (2017).
- [22] M. Oi, *Phys. Rev. C* **76**, 044308 (2007).
- [23] N. Lyutorovich, V. Tselyaev, J. Speth, G. Martinez-Pinedo, K. Langanke, and P.-G. Reinhard, *Phys. Rev. C* **105**, 014327 (2022).
- [24] V. Tselyaev, N. Lyutorovich, J. Speth, and P.-G. Reinhard, *Phys. Rev. C* **97**, 044308 (2018).
- [25] A. I. Vdovin and V. G. Soloviev, *Sov. J. Part. Nucl.* **14**, 99 (1983).
- [26] V. V. Voronov and V. G. Soloviev, *Sov. J. Part. Nucl.* **14**, 583 (1983).
- [27] V. G. Soloviev, *Theory of Atomic Nuclei: Quasiparticles and Phonons* (Institute of Physics, Bristol and Philadelphia, 1992).
- [28] C. A. Bertulani and V. Yu. Ponomarev, *Phys. Rep.* **321**, 139 (1999).
- [29] N. Van Giai, C. Stoyanov, and V. Voronov, *Phys. Rev. C* **57**, 1204 (1998).
- [30] A. P. Severyukhin, S. Åberg, N. N. Arsenyev, and R. G. Nazmitdinov, *Phys. Rev. C* **98**, 044319 (2018).
- [31] F. Andreozzi, F. Knapp, N. Lo Iudice, A. Porrino, and J. Kvasil, *Phys. Rev. C* **75**, 044312 (2007).
- [32] D. Bianco, F. Knapp, N. Lo Iudice, F. Andreozzi, and A. Porrino, *Phys. Rev. C* **85**, 014313 (2012).
- [33] G. De Gregorio, F. Knapp, N. Lo Iudice, and P. Veselý, *Phys. Rev. C* **93**, 044314 (2016).
- [34] E. Litvinova, *Phys. Rev. C* **91**, 034332 (2015).
- [35] V. Tselyaev, N. Lyutorovich, J. Speth, and P.-G. Reinhard, *Phys. Rev. C* **102**, 064319 (2020).
- [36] N. Lyutorovich, V. Tselyaev, J. Speth, S. Krewald, and P.-G. Reinhard, *Phys. At. Nucl.* **79**, 868 (2016).
- [37] P. Klüpfel, J. Erler, P. . G. Reinhard, and J. A. Maruhn, *Eur. Phys. J. A* **37**, 343 (2008), <http://www.arxiv.org/abs/0804.340>.
- [38] M. Martin, *Nuclear Data Sheets* **108**, 1583 (2007).
- [39] A. Heusler, *Journal of Physics: Conference Series* **1643**, 012137 (2020).
- [40] S. Basu and E. Mccutchan, *Nuclear Data Sheets* **165**, 1 (2020).
- [41] A. Heusler, R. V. Jolos, T. Faestermann, R. Hertenberger, H.-F. Wirth, and P. von Brentano, *Phys. Rev. C* **93**, 054321 (2016).